COBEM 2021 26th International Congress of Mechanical Engineering
November 22-26, 2021, Virtual Congress, Brazil

THEORETICAL ANALYSIS OF AN OIL COOLER PIPE FOR THE THERMAL MANAGEMENT OF HERMETIC COMPRESSORS

Thiago Dutra
André M. da Silva
TEG Thermofluids Engineering Group - Universidade Federal de Santa Catarina, Rov. Gov. Jorde Lacerda, 3201 Jardim das Avenidas, Araranguá - SC
thiago.dutra@teg.ufsc.br, andremachado1996@outlook.com

Abstract. *Hermetic compressors have been designed in smaller dimensions and to operate in wider application envelopes. As a result, the temperature of internal components increases during operation and thermal management solutions are needed to avoid superheating of critical components, such as the electric motor. This paper presents a theoretical analysis to assess the effect of an oil cooler pipe (OCP) on the reduction of the electric motor temperature. Refrigerant fluid flows from the exit of the condenser straight through the OCP, removing heat from the lubricant oil sump inside the compressor, and cooling the electric motor. A simulation model was developed by coupling a lumped-parameter thermal model of a hermetic reciprocating compressor with a theoretical model for the heat transfer in the OCP. The compressor thermal model was validated with temperature measurements obtained from a compressor adopted for household and light commercial applications. Results show that the motor temperature decreases at the expense of a reduction in the cooling capacity, which indicates a tradeoff between compressor reliability and refrigeration system performance. Moreover, the benefit of the OCP was found to decrease at high condensing temperatures. Due to that, an additional expansion device was included in the line between the condenser and the OCP to control the inlet temperature in the latter. Several analyses were carried out with this new configuration and its impact on the motor temperature and system performance was evaluated.*

Keywords: *hermetic compressor, thermal management, simulation model*

1. INTRODUCTION

One of the main drivers of refrigeration systems design is cost. Due to that, the hermetic compressors usually adopted in these applications have been miniaturized and made to operate under stretched application envelopes. As a consequence, high energetic densities arise in these compressors, bringing about an increase of the temperature of the internal components. In particular, the increase of the electric motor temperature may lead to reliability problems, especially if this temperature surpass the maximum allowed temperature for the electric insulator class, causing a deterioration of the insulator and a decrease of the motor life span (Pyrhonen et al., 2013). Thermal management alternatives that ensure the electric motor temperature in an acceptable range need to be assessed and thermal simulation models fit to this purpose.

There are many papers in the literature concerning the development of thermal simulation models for hermetic compressors. In lumped-parameter models, the energy conservation equation is applied to control volumes associated with compressor components. Thermal conductances between components are set using experimental data (Meyer and Thompson, 1990; Diniz et al., 2019) or heat transfer correlations (Ooi, 2003; Zhang et al., 2020). Ooi (2003) used a thermal-model to quantify the effect of suction muffler modifications on the suction gas temperature and, as a result, on the compressor efficiency. Dutra and Deschamps (2015a and 2015b) adopted a thermal simulation model for a hermetic reciprocating compressor to assess the influence of operating conditions and geometric parameters on the electric motor temperature. Recently, Dutra and Moratelli (2019) presented a theoretical simulation model for optimization of fins on the shell of a hermetic compressor, with the objective of reducing the electric motor temperature.

Some studies have been reported in the literature concerning the development of distributed-parameter models for the thermal simulation of compressors (Wu et al., 2016; Oliveira et al., 2017; Posch et al., 2018a). These models provide a fine spatial resolution of the temperature distribution at the expense of high computational cost. Oliveira et al. (2017) used a commercial software based on the finite volume method to perform a thermal simulation of an oil-free linear compressor. The model was used to evaluate how the insulating gasket at the compressor head affects the compressor efficiency. Posch et al. (2018a) developed a distributed-parameter thermal model for a hermetic compressor and used it to assess the effect of a heat sink at the valve plate on the suction gas superheating degree, which affects the compressor efficiency. Wu et al. (2016) performed a three-dimensional thermal simulation of a rotary compressor to compute the temperature distribution in the electric motor. The model considered the presence of the air gap between the rotor and the stator, as well as the influence of the rotating balancer attached to the rotor on the fluid field and the impact of the insulation material on the heat transfer.

In spite of several works related to thermal modeling of hermetic compressors, there is still room for researching different strategies for compressor thermal management, specially associated with the electric motor. According to many papers in the literature (Dutra and Deschamps, 2013; Posch et al., 2018b), further the lubrication and sealing functions, the lubricant oil plays an important role on the compressor cooling, transporting heat from the hot components to the shell. Usually, a centrifugal oil pump coupled to the crankshaft is adopted to suck oil from an oil sump at the bottom of the shell and takes it to the compressor bearings. Part of the oil is expelled through an upper groove of the crankshaft, hitting the upper part of the shell and returning to the oil sump by flowing through internal components and the shell (Posch et al., 2018b).

The bottleneck of the compressor heat rejection is the high thermal resistance between the shell and the air outside, which is due to low-velocity forced convection. Dutra and Moratelli (2019) performed an evaluation of fins attached to the shell to decrease such a thermal resistance and, as a result, the temperature of compressor internal components, especially of the electric motor. Since the lubricant oil has a recognized importance on the compressor heat distribution, another potential thermal management solution would raise from removing heat straight from the oil. This could be done by using the refrigerant fluid after leaving the condenser, and making it to flow through an oil cooler pipe (OCP) positioned in the oil sump at the bottom of the compressor shell.

This paper presents a theoretical analysis to evaluate the effect of an OCP on the reduction of the electric motor temperature of a hermetic compressor used in refrigeration. A simulation model formed by the integration of a compressor lumped-parameter thermal model with a theoretical model for the heat transfer in the OCP is adopted to this purpose. Before coupling the models, the thermal model is validated with experimental data. The integrated model is employed then to analyze the effect of operating condition, OCP temperature and OCP length on the electric motor temperature and on the refrigeration capacity.

2. OCP CONCEPT

The OCP is a pipe that is placed in the lubricant oil sump and through which refrigerant fluid flows after leaving the condenser (Figure 1a). The temperature of the lubricant oil is commonly higher than the condensing temperature and, as a result, the lubricant oil rejects heat to the OCP, bringing about an increase of the vapor quality and its enthalpy. Such an increase of enthalpy leads to a reduction of the system refrigeration capacity ($h_4 - h_3$), as represented in the pressure-enthalpy diagram at Figure 1b. One should note that the refrigerant thermodynamic state at the outlet of the condenser is assumed saturated liquid, that the pressure drop through the heat exchangers is neglected and that the throttling process is isenthalpic.

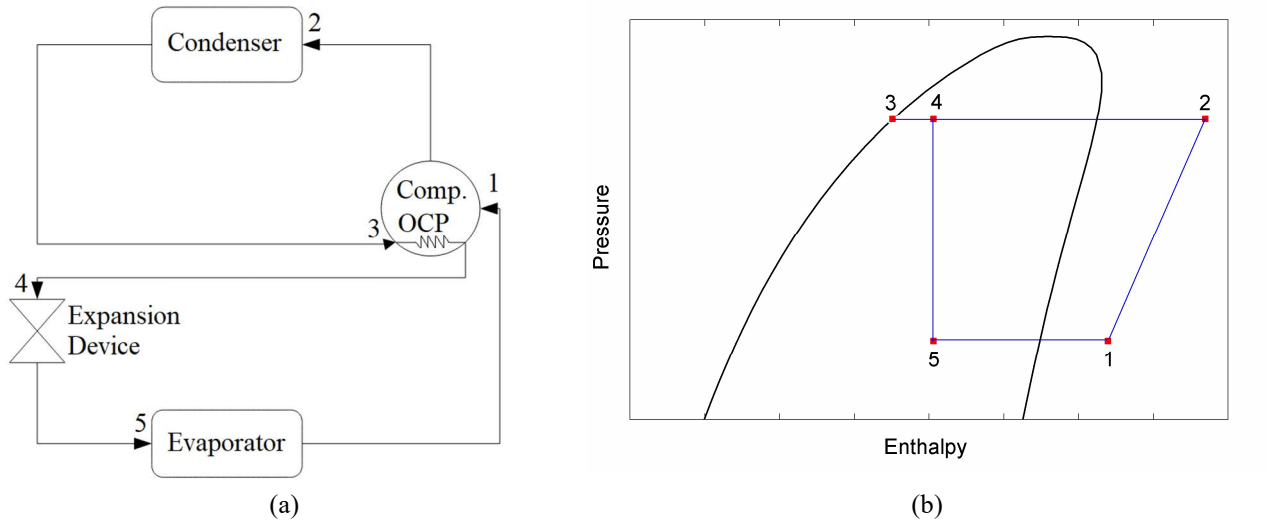

(a) (b)

Figure 1. (a) Schematic of a refrigeration system with the OCP and (b) referred pressure-enthalpy diagram.

An additional expansion device may be included at the OCP inlet to control the refrigerant temperature in the OCP (from herein after called OCP temperature). This might be an interesting configuration since a lower OCP temperature can be set, increasing the heat transfer rate and decreasing the electric motor temperature. Figure 2 shows a schematic of the refrigeration system with this additional expansion device and the pressure-enthalpy diagram referred to this configuration.

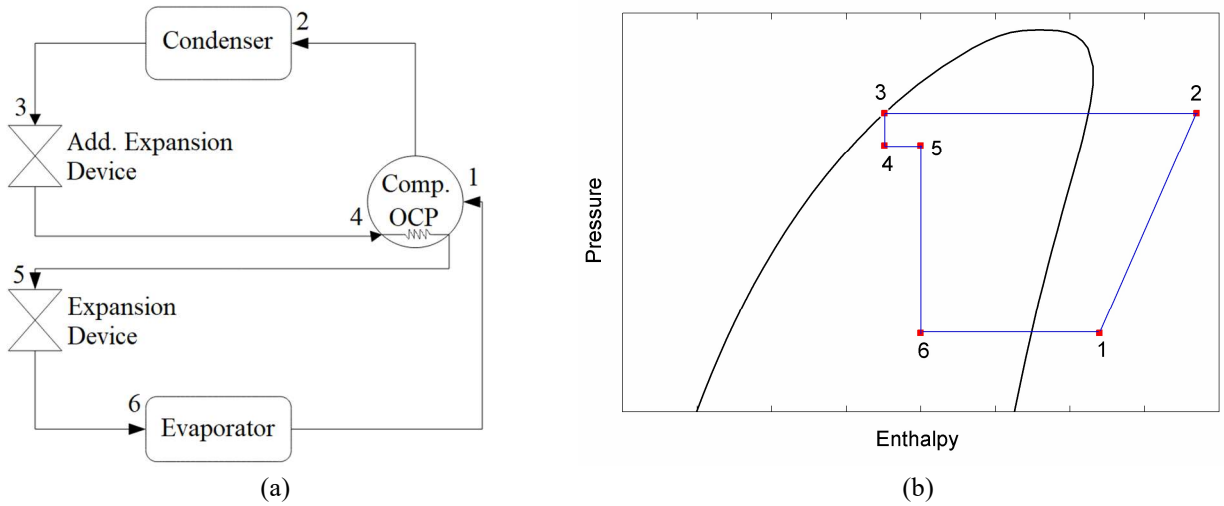

Figure 2. (a) Schematic of a refrigeration system with the OCP and additional expansion device and (b) referred pressure-enthalpy diagram.

3. SIMULATION MODEL

The simulation model is formed by the combination of a lumped-parameter thermal model for the compressor and a distributed-parameter thermal model for the OCP. These models are presented separately in the next sections.

3.1 Compressor thermal model

The thermal model proposed herein is similar to that presented by Dutra and Deschamps (2015b), but with some modifications to take into account the heat transfer through the lubricant oil. As shown in Figure 3, the compressor is divided into nine lumped elements: suction muffler (1), compression chamber (2), discharge chamber (3), discharge muffler (4), discharge tube (5), electric motor (6), internal environment (7), shell (8) and lubricant oil (9). The steady-state formulation of the energy equation is applied to each one of them:

$$\dot{Q}_i - \dot{W}_i = \sum(\dot{m}h)_{i,out} - \sum(\dot{m}h)_{i,in} \tag{1}$$

where $\dot{Q}_i$ stands for the convective heat transfer rate between the element i and its surroundings, $\dot{W}_i$ is the rate of work through the control surfaces of element i, and $\Sigma(\dot{m}h)_{i,in}$ and $\Sigma(\dot{m}h)_{i,out}$ represent the energy transfer rate between element i and upstream and downstream chambers, respectively. Potential and kinetic energy variations were neglected in Eq. (1).

Table 1 summarizes all the energy balances considered in the compressor thermal model. The compression process is modeled as adiabatic, with no backflow and leakage. The indicated power, $\dot{W}_{ind}$, is computed as follows:

$$\dot{W}_{ind} = \eta_{ele}\dot{W}_{ele} - \dot{Q}_b \tag{2}$$

where $\dot{W}_{ele}$ is the power input, η_{ele} is the electric motor efficiency and $\dot{Q}_b$ denotes the bearings friction losses. The power input and the mass flow rate are computed from isentropic and volumetric efficiencies, η_s and η_v, as follows:

$$\dot{W}_{ele} = \frac{\dot{m}(h^s - h_{sl})}{\eta_s}; \qquad \dot{m} = \eta_v \rho_{sl} V_{sw} f \tag{3}$$

where ρ_{sl} and h_{sl} are the gas density and specific enthalpy evaluated at the evaporating pressure and suction line temperature, respectively, and h^s is the specific enthalpy computed with the condensing pressure and suction line specific entropy. The swept volume is denoted by V_{sw} and the line frequency is f. The electric motor efficiency as well as the isentropic and volumetric efficiencies and the bearings friction losses are obtained from data available in Dutra and Deschamps (2015b). Additional relations are necessary to close the non-linear system of equations described in Table 1:

$$T_1 = 0.5(T_{sl} + T_{sc}); \qquad T_4 = 0.5(T_3 + T_{dm}); \qquad T_5 = 0.5(T_{dm} + T_{dl}) \tag{4}$$

being T_1, T_4 and T_5 averages of inlet and outlet temperatures in each control volume. The Newton-Raphson technique is applied to solve the non-linear system of equations, implemented in an in-house code written in MATLAB.

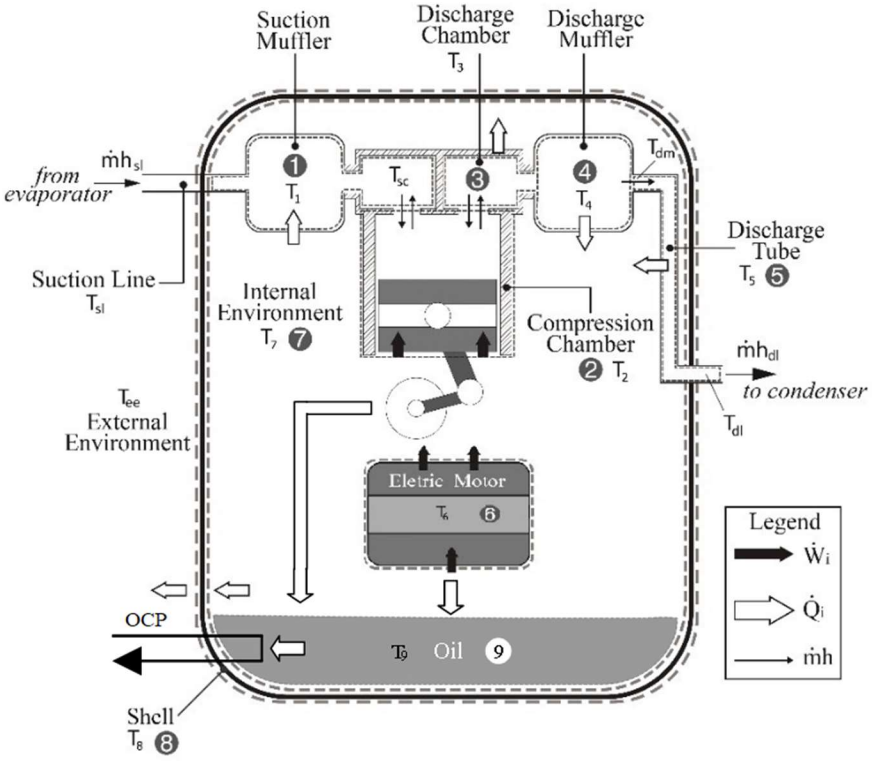

Figure 3. Schematic of the compressor lumped elements.

Table 1. Energy balance terms applied to the lumped elements.

ID	$\dot{Q}_i$	$\dot{W}_i$	$\sum(\dot{m}h)_{i,in}$	$\sum(\dot{m}h)_{i,out}$
1	$UA_{1,7}(T_1 - T_7)$	-	$\dot{m}h_{sl}$	$\dot{m}h_{sc}$
2	-	$\dot{W}_{ind}$	$\dot{m}h_{sc}$	$\dot{m}h_2$
3	$UA_{3,7}(T_3 - T_7)$	-	$\dot{m}h_2$	$\dot{m}h_3$
4	$UA_{4,7}(T_4 - T_7)$	-	$\dot{m}h_3$	$\dot{m}h_{dm}$
5	$UA_{5,7}(T_5 - T_7)$	-	$\dot{m}h_{dm}$	$\dot{m}h_{dl}$
6	$UA_{6,9}(T_6 - T_9)$	$\dot{W}_{ele}(1 - \eta_{ele})$	-	-
7	$\sum_1^8 UA_{i,7}(T_7 - T_i)$; for i≠ 2; 6; 7	-	-	-
8	$UA_{8,ee}(T_8 - T_{ee}) + UA_{8,7}(T_8 - T_7) + UA_{8,9}(T_8 - T_9)$	-	-	-
9	$UA_{6,9}(T_9 - T_6) + UA_{8,9}(T_9 - T_8) + \dot{Q}_b - \dot{Q}_{ocp}$	-	-	-

Still regarding Table 1, one notices that all the heat generated due to the electromechanical energy conversion and the friction losses in bearings is assumed to be rejected to the lubricant oil, since the oil flows over the crankcase and the electric motor. In the energy balance associated with the lubricant oil, the heat transfer rate released to the OCP is denoted by $\dot{Q}_{ocp}$ and is computed with the OCP model. Thermal conductances between generic elements i and j, $UA_{i,j}$, were obtained using experimental data for two operating conditions represented by pairs of evaporating and condensing temperatures, T_e and T_c: (i) T_e = -35.0 °C/T_c = 54.4 °C and (ii) T_e = -10.0 °C/ T_c = 54.4 °C. The least squares method was adopted to establish linear relationships between $UA_{i,j}$ and T_e, i.e. $UA_{i,j} = c_1 + c_2 T_e$, in which c_1 and c_2 are the fitted coefficients.

3.2 OCP model

The oil cooler pipe model is based on a distributed-parameter steady-state formulation of the energy conservation equation, disregarding the rate of work and variations on the kinetic and potential energy terms (Figure 4):

$$\delta\dot{Q} = \dot{m}h_{lv}(x_{out} - x_{in}) \tag{5}$$

in which h_{lv} represents the latent heat of vaporization evaluated at the temperature of the refrigerant in the OCP, T_{ocp}, and x_{out} and x_{in}, stand for the vapor quality in the inlet and outlet of the control volume, respectively. The pipe of length L and diameter D is divided into n equal parts of length $\Delta z = L/n$. By default, the thermodynamic state at the OCP inlet is set as saturated liquid ($x = 0$) at the condensing temperature, T_c, which is defined by the operating condition. The heat transfer rate term $\delta\dot{Q}$ in a portion of length Δz is given by:

$$\delta\dot{Q} = U\pi D\Delta z\left(T_9 - T_{ocp}\right) \tag{6}$$

where U is the global heat transfer coefficient between the lubricant oil sump and the refrigerant in the OCP. Neglecting conduction and fouling thermal resistances, U is computed as:

$$U = \frac{H_{ocp,i}H_{ocp,e}}{H_{ocp,i} + H_{ocp,e}} \tag{7}$$

in which $H_{ocp,e}$ and $H_{ocp,i}$ denotes the OCP external and internal heat transfer coefficients, respectively. The former is calculated with a traditional correlation for external flow past a circular cylinder (Zukauskas, 1972):

$$H_{ocp,e} = \frac{k_{oil}}{D}0.26Re^{0.6}Pr^{0.36}\left(\frac{Pr}{Pr_w}\right)^{0.25} \tag{8}$$

being k_{oil}, Re and Pr, the thermal conductivity of the lubricant oil, the Reynolds and the Prandtl numbers, respectively. Characteristic length and velocity for Reynolds number evaluation are the tube diameter D and the tangential velocity of the centrifugal pump immersed into the lubricant oil sump. All properties are computed with the film temperature, using relationships adopted from Mermond (1999), except Pr_w that is evaluated with the OCP wall temperature.

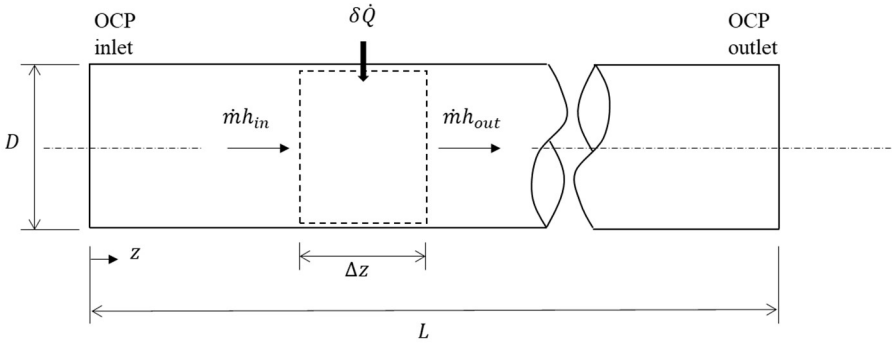

Figure 4. OCP schematic.

The heat transfer coefficient in the internal side of the OCP is assessed via a correlation proposed by Shah (1982), which takes into account the effects of both nucleate boiling and convective boiling. To that extent, the dimensionless parameters convective number, Co, boiling number, Bo, and Froude number, Fr, are obtained as follows:

$$Co = \left(\frac{1-x}{x}\right)^{0.8}\left(\frac{\rho_v}{\rho_l}\right)^{0.5} \tag{9}$$

$$Bo = \frac{U\left(T_9 - T_{ocp}\right)}{Gh_{lv}} \tag{10}$$

$$Fr = \frac{G^2}{\rho_l^2 gD} \tag{11}$$

where ρ_v and ρ_l are the saturated vapor and saturated liquid mass densities of the refrigerant evaluated at T_{ocp}, G is the mass flow rate per unit area ($=4\dot{m}/\pi D^2$) and g is the gravitational acceleration. The OCP internal side heat transfer coefficient is determined by:

$$H_{ocp,i} = \varphi(Co, Bo, Fr) H_{lo} \tag{12}$$

where φ is a function that assumes different forms, depending on the boiling regime and H_{lo} is the heat transfer coefficient estimated via the Dittus-Boelter equation for a liquid only turbulent flow in the OCP. Further details of the method employed to determine $H_{ocp,i}$ should be consulted in Shah (1982). As the vapor quality at the outlet of a control volume is calculated, this value is assigned as the vapor quality at the inlet of the adjacent control volume and the calculation is replicated. The solution advances following this procedure until the OCP outlet is reached. Finally, the heat transfer rate through the OCP is computed as:

$$\dot{Q}_{ocp} = \dot{m}\left(h_{out,ocp} - h_{in,ocp}\right) \tag{13}$$

being $h_{in,ocp}$ and $h_{out,ocp}$ the specific enthalpies at the inlet and the outlet of the OCP, respectively. The former is evaluated as saturated liquid ($x = 0$) at the condensing pressure and the latter is computed with the OCP model.

3.3 Simulation procedure

First of all, the operating condition is established (T_e, T_c, f, T_{ee} and T_{sl}), the input data are set, including electric motor efficiency, volumetric and isentropic efficiencies, as well as the thermal conductance relationships $UA_{i,j} = f(T_e)$. Initial guesses are set for the compressor temperature distribution, T_o, and the heat transfer rate through the OCP, $\dot{Q}^o_{ocp}$. The thermal model is run and the temperature distribution is calculated. The lubricant oil temperature is supplied as input data for the OCP model, which is executed and a new value for $\dot{Q}_{ocp}$ is calculated. If the deviation between two consecutive computations for $\dot{Q}_{ocp}$ is lower than 0.001 W, convergence is achieved and the simulation is finished. Otherwise, the updated value for $\dot{Q}_{ocp}$ is supplied as input data to the thermal model and all the calculations are repeated. Figure 5 presents the flowchart of the simulation procedure.

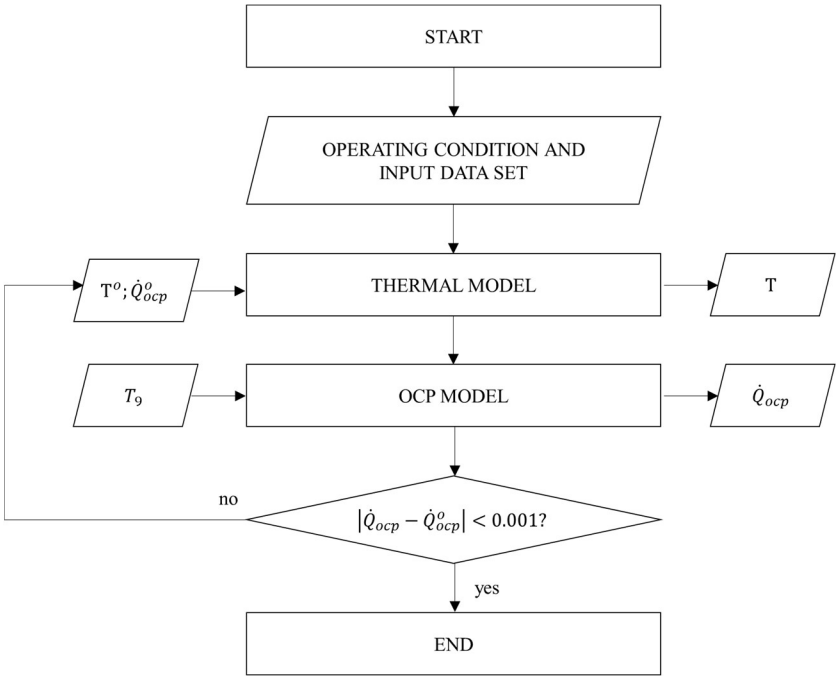

Figure 5. Simulation flowchart.

4. RESULTS

All the results presented in this section were obtained for a 50 Hz small reciprocating compressor adopted for household and light commercial refrigeration applications. The compressor swept volume is 5.5 cm³ and the refrigerant fluid is propane (R290). The outside air and the suction line temperatures (T_{ee} and T_{sl}) were both set to 32°C.

4.1 Thermal model validation

The compressor thermal model is validated using experimental data provided by Dutra and Moratelli (2019). Predictions of motor temperature are compared with measurements under a wide range of operating conditions formed by combinations of three evaporating temperatures (T_e = -35.0 °C; -23.3 °C; -10.0 °C) and three condensing temperatures (T_c = 45.0 °C; 54.4 °C; 70.0 °C). According to Fig. 6, when the operating condition is -35.0 °C/54.4 °C or -10.0 °C/54.4 °C, predictions are found to exactly match measurements, since the thermal model is adjusted with data from these conditions. Good agreement is also observed on the remaining conditions, with a maximum deviation of 1.5°C between computations and experimental data. Measurements accuracy is ± 2 °C with a 95% confidence interval.

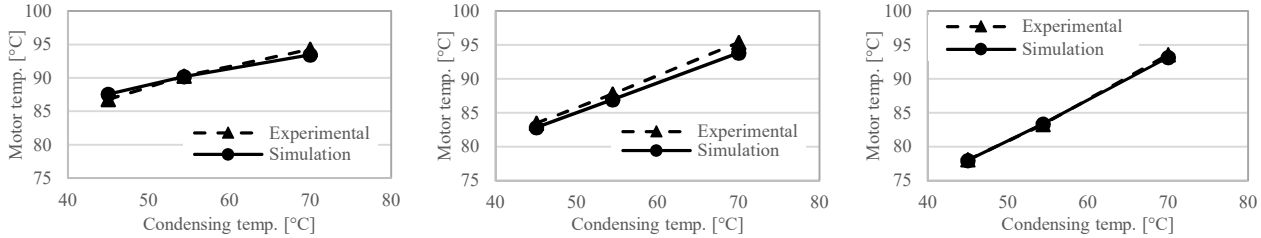

(a) T_e = -35.0°C (b) T_e = -23.3°C (c) T_e = -10.0°C

Figure 6. Motor temperature as a function of evaporating and condensing temperatures.

4.2 Effect of the operating condition

Once the compressor thermal model is validated, it is coupled to the OCP model. A 6.35 mm diameter -100 mm length circular pipe was considered for the analyses in this stage. Simulations were carried out under the same aforementioned operating conditions. Figure 7a shows the motor temperature drop (ΔT_6) as a result of the OCP utilization at different pairs of evaporating and condensing temperatures. The higher the condensing temperature, the lower the decrease in the motor temperature, since the lower is the difference between the lubricant oil temperature (T_9) and the OCP temperature ($T_{ocp} = T_c$). Such a temperature difference is around 7 °C and 16 °C when the condensing temperature is 70 °C and 45 °C, respectively.

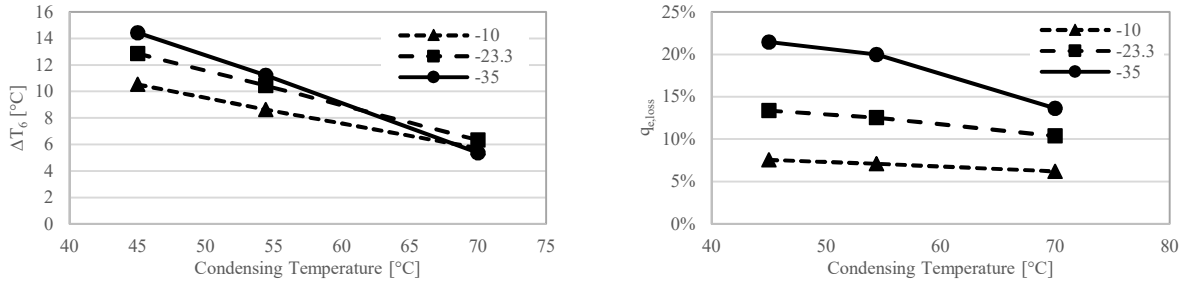

(a) (b)

Figure 7. (a) Motor temperature reduction and (b) refrigeration capacity loss as a function of the operating condition.

The motor temperature is reduced at the expense of the refrigeration capacity loss (Figure 7b) computed as

$$q_{e,loss} = \frac{h_{out,ocp} - h_{in,ocp}}{h_{sl} - h_{in,ocp}} \times 100. \tag{14}$$

One notices that the refrigeration capacity loss is increased with the decrease of the evaporating temperature. The lower the evaporating temperature, the lower the mass flow rate supplied by the compressor and the higher the enthalpy change in the OCP ($h_{out,ocp} - h_{in,ocp}$), for a roughly constant $\dot{Q}_{ocp}$. As a result, the lower is the refrigeration effect ($h_{out,ocp}$ - h_{sl}) and therefore the refrigeration capacity provided by the evaporator. Moreover, the refrigeration capacity loss increases as the condensing temperature decreases due to the intensification of the heat transfer led by the increase of T_9 - T_{ocp}.

The OCP performs worse at those operating conditions in which the motor temperature is higher (T_c = 70 °C). For instance, the motor temperature decreases only by 5.5 °C (Figure 7a) at -35 °C/ 70 °C, when the motor temperature is 93.5 °C in baseline configuration (Figure 6a). On the other hand, the motor temperature drops 14.5 °C (from 87.6 °C to 73.1 °C) at -35 °C/ 45 °C. This problem is circumvented by including an additional expansion device at the refrigeration circuit, throttling the refrigerant at the inlet of the OCP (Figure 2).

3.3 Effect of the OCP temperature

Figures 8a and 8b present results of motor temperature drop and refrigeration capacity loss, respectively, as a function of the OCP temperature for two operating conditions: -35 °C/ 70 °C and -10 °C/ 70 °C. The motor temperature drop increases similarly for both operating conditions as reducing the OCP temperature and is around 12 °C when T_{ocp} = 55 °C. However, such a temperature drop in the electric motor is attained with an increase in the refrigeration capacity loss of 30 % and 14 % (Figure 8b), for the operating conditions -35 °C/ 70 °C and -10 °C/ 70 °C, respectively. Thus, one concludes that the OCP thermal management solution performs better at high evaporating temperatures and so is more likely to be applied under these conditions.

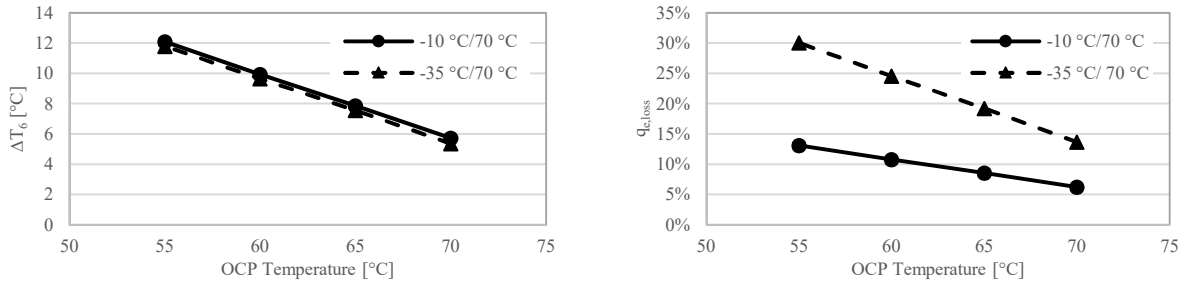

Figure 8. (a) Motor temperature reduction and (b) refrigeration capacity loss as a function of the OCP temperature.

3.4 Effect of the OCP length

The OCP length was varied between 0.05 m and 0.35 m and its impact on the motor temperature and the refrigeration capacity loss is shown in Figures 9a and 9b. Results were obtained at two operating conditions, namely -35 °C / 70 °C and -10 °C / 70 °C. According to Figure 9a, as the OCP length is increased, a greater heat transfer area is made available, increasing the motor temperature drop. However, $\Delta T6$ tends to an asymptotic value, since the temperature difference $T_9 - T_{ocp}$ decreases asymptotically as well. Moreover, the adoption of a 0.35 m length OCP brings about reductions of 9 °C and 7.8 °C in the motor temperature at -10 °C / 70 °C and -35 °C / 70 °C, respectively, which are due to reductions of 20.7 % and 9.8 % of the refrigeration capacity at these operating conditions (Figure 9b). Again, such an outcome indicates the OCP performs better at a high evaporating temperature operating condition.

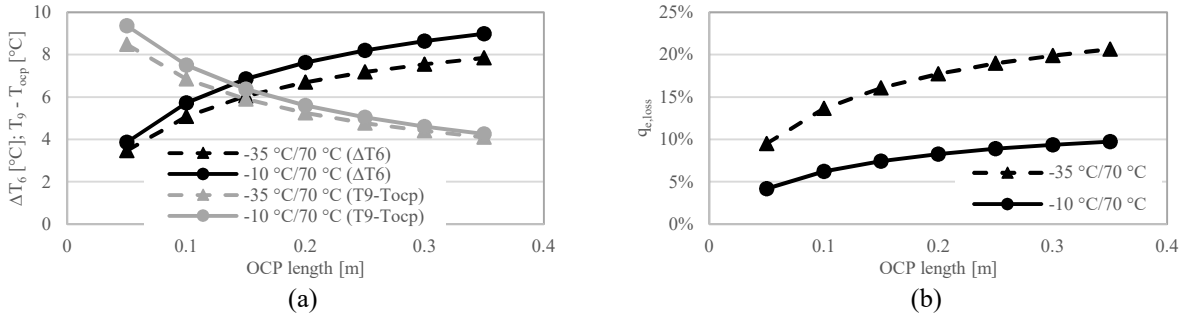

Figure 9. (a) Motor temperature reduction and (b) refrigeration capacity loss as a function of the OCP length and evaporating temperature.

5. CONCLUSION

This paper presented a theoretical analysis to evaluate the effect of an oil cooler pipe on the reduction of the electric motor temperature of a hermetic compressor adopted for refrigeration applications. A simulation model formed by the integration of a compressor lumped-parameter thermal model with a theoretical model for the heat transfer in the OCP was implemented to this purpose. The compressor thermal model was validated with experimental data before being coupled to the OCP model. It was concluded that the higher the condensing temperature the worse the OCP performs. Such a difficulty was circumvented by throttling the refrigerant with an additional expansion device at the inlet of the OCP, to control the OCP temperature. As a result, the motor temperature drop increased from 5.5 °C to 12 °C, as the OCP temperature is controlled at 55 °C under a condensing temperature of 70 °C. Finally, it was found that the motor temperature drop increases asymptotically as the OCP length is incremented and that the OCP is likely to be adopted under high evaporating temperature, since the refrigeration capacity loss is lower under these operating conditions.

6. REFERENCES

Diniz, M. C., Hermes, C. J. L., Deschamps, C. J., 2019. "Transient simulation of small-capacity reciprocating compressors in on-off controlled refrigerators". *International Journal of Refrigeration*, Vol. 102, pp. 12–21.

Dutra, T., Deschamps, C. J., 2013. "Experimental characterization of heat transfer in the componentsof a small hermetic reciprocating compressor". *Applied Thermal Engineering*, Vol. 58, pp. 499–510.

Dutra, T., Deschamps, C. J., 2015a. "A thermal network model for induction motors of hermetic reciprocating compressors". *IOP Conf. Ser.: Mater. Sci. Eng.* 90 012020.

Dutra, T., Deschamps, C. J., 2015b. "A simulation approach for hermetic reciprocating compressors including electrical motor modeling". *International Journal of Refrigeration,* Vol. 59, pp. 168-181.

Dutra, T., Moratelli, S., 2019. "A theoretical simulation model for optimization of fins on the shell of a hermetic reciprocating compressor". *IOP Conf. Ser.: Mater. Sci. Eng.* 604 012028.

Mermond, Y., Feidt, M., Marvillet, C., 1999. "Propriétés thermodynamiques et physiques des mélanges de fluides frigorigènes et d'huiles". *International Journal of Refrigeration,* Vol. 22, pp. 569-579.

Meyer, W. A., Thompson, H. D., 1990. "An analytical model of heat transfer to the suction gas in a low-side hermetic refrigeration compressor". *Proc. Int. Compress. Eng. Conf. at Purdue*. West Lafayette, USA, pp. 898–907.

Oliveira, M. J., Diniz, M. C., Deschamps, C. J., 2017. "Predicting the temperature distribution and the suction gas superheating of an oil-free linear compressor". *Journal of Process Mechanical Engineering*. 231 (1) pp. 47-56.

Ooi, K. T., 2003. "Heat transfer study of a hermetic refrigeration compressor". *Applied Thermal Engineering*, Vol. 23, pp. 1931-1945.

Posch, S., Hopfgartner, J., Dür, L., Eichinger, M., Stangl, S., Almbauer, R., 2018a. "Thermal loss analysis of hermetic compressors using numerical simulation". *Applied Thermal Engineering*, Vol. 130, pp. 1580–1589.

Posch, S., Hopfgartner, J., Berger, E., Zuber, B., Shöllauf, P., Almbauer, R., 2018b. "Numerical analysis of a hermetic reciprocating compressor oil pump system". *International Journal of Refrigeration*, Vol. 85, pp. 135–143.

Pyrhonen, J., Jokinen, T., Hrabovcova, V., 2013. *Design of Rotating Electrical Machines*. John Wiley & Sons.

Shah, M. M., 1982. "Chart correlation for saturated boiling heat transfer: equation and further study". *ASHRAE Transactions*, Vol. 88 (1), pp. 185-196.

Wu, J., Hu, J., Chen, A., Mei, P., Zhou, X., Chen, Z., 2016. "Numerical analysis of temperature distribution of motor-refrigerant in a R32 rotary compressor". *Applied Thermal Engineering*, Vol. 95, pp. 365-373.

Zhang, X., Ziviani, D., Braun, J. E., Groll E. A., 2020. "Theoretical analysis of dynamic characteristics in linear compressors". *International Journal of Refrigeration*, Vol. 109, pp. 114–127.

Zukauskas, A., 1972. "Heat transfer from tubes in crossflow". *Advances in Heat Transfer*, Vol. 8, pp. 93-160.

7. RESPONSIBILITY NOTICE

The authors are the only responsible for the printed material included in this paper.